JOURNAL OF SOLID STATE CHEMISTRY 72, 201–208 (1988)

Photoelectrochemical Study of a Spinel-Type Titanomagnetite

B. TEUNG CHANG,* MOHAMED JAKANI, GUY CAMPET, AND JEAN CLAVERIE†

Laboratoire de Chimie du Solide du CNRS, Université de Bordeaux I, 351, cours de la Libération, 33405 Talence Cédex, France

Received November 13, 1985; in revised form January 26, 1987

The electrical and photoelectrical properties of spinel-type titanomagnetite $Fe_{3-x}Ti_xO_4$ with $x = 0.964$ have been investigated. The electrical conductivity involves a mechanism by which electrons in octahedral sites hop from the $Fe^{2+}: t_{2g\beta}$ level to the $Fe^{3+}: t_{2g\beta}$ level, despite the observed positive value of the Seebeck coefficient. The photoelectrode shows significant anodic photocurrent and negative flatband potential which are evidence of an *n*-type character. The flatband potential determined from impedance measurements is found to be close to that of *n*-type α-Fe_2O_3. In addition, the photocurrent is due to indirect electronic transitions occurring at 2.00 and 2.39 eV. A proposed energy level diagram suggests that the photoresponse results from either iron–iron or (and) iron–titanium charge transfers.

Introduction

Among the various metal oxides, iron oxide is apparently a potentially suitable electrode for photoelectrochemical energy conversion because of its relatively low energy bandgap value ($Eg \simeq 2.2$ eV) and its excellent chemical stability in both acidic and alkaline electrolytes (*1–4*). It does, however, suffer from the disadvantage of low quantum efficiency, resulting from a low absorption coefficient (α), small carrier mobilities (μ), and a low faradic rate constant at the surface (*2, 5, 6*). Some attempts to improve the efficiency have been made by various methods, such as doping with other metal oxides (e.g., TiO_2, SnO_2) (*7, 8*) or using thin film electrodes (*9*) or heterojunction electrodes (*10–13*). According to those previous investigations it appears that the combination of iron oxide and titanium oxide, either through doping or heterojunction, leads to a strong improvement in the iron oxide photoanode. In this line, Morosin *et al.* have shown that the photoconduction mechanism of iron–titanium oxide electrodes is conditioned by the respective structural arrangements of the iron and titanium "chromophores" in pseudobrookite or spinel-type structures (*14*): because of the presence of disordered metal sites, photoconduction paths can then be found in all directions that involve only iron atoms. They correspond to a energy bandgap of only 2.2 eV.

On the other hand the presence of titanium in electrode materials generally con-

* Permanent address: Department of Chemistry, Faculty of Science, Korea University, Kodaira, Tokyo 187, Japan.

† To whom correspondence should be addressed.

0022-4596/88 $3.00

tributes to a reduction in electron affinity and thus in flatband potential (*15*). Thus, the spinel-type structure of Fe_2TiO_4 should contribute, in particular, to both small energy gap and low electron affinity, two features generally contradictory in oxide-type electrodes.

Unfortunately, stoichiometric Fe_2TiO_4 is a very poor conductor and thus cannot be utilized as an electrode in a photoelectrochemical cell (*16*). Ginley et al., however, observed a conductivity of 10^{-1} to 10^{-2} Ω^{-1} cm^{-1} for a Fe_2TiO_4 sample resulting from heating of the samples at high temperature under vacuum which causes small deviations from stoichiometry (*15*). According to these authors the stoichiometry is actually not well controlled and the flatband potential is quite sensitive to the exact composition. As a consequence the V_{fb} values measured for Fe_2TiO_4 should not be reliable.

On the contary, a reproducible conductivity should be expected for Fe_2TiO_4 after doping with Fe^{3+}. From this viewpoint the spinel-type solid solution Fe_2TiO_4–Fe_3O_4 seemed to be appropriate as it allows measurements for well-defined compositions. The present paper is devoted mainly to detailed investigations of the electrical and photoelectrochemical properties of a titanium-rich spinel-type crystal with nominal composition $Fe_{2.036}Ti_{0.964}O_4$ (such spinels with a formula close to Fe_2TiO_4 are sometimes called ulvospinels).

Experimental

Crystals of ulvospinel were kindly provided by H. Harrison, Purdue University. Crystals with a nominal composition of 3.6 atom% magnetite (Fe_3O_4) and 96.4 atom% Fe_2TiO_4 were grown under a reductive atmosphere of 15% CO_2 and 85% CO by the skull melting technique (*17*). Each crystal cut from the original boule was characterized by X-ray diffraction and electron microprobe analyses. Its actual composition is very close to the expected nominal one, $Fe_{2.036}Ti_{0.964}O_4$. The X-ray diffraction pattern agrees clearly with a spinel-type structure.

Electrical conductivity (σ) and thermoelectric power (θ) were measured in the temperature ranges 95–290 and 180–290 K, respectively. Methods and equipment used are described elsewhere (*18*).

The samples used for electrochemical and photoelectrochemical measurements were polished with SiC emery paper, diamond, and alumina powders, and then chemically etched in HNO_3:HF:CH_3COOH (5 : 3 : 3) for 1 min.

Electrical contact was obtained on the back surface with an In–Ga alloy. Then a copper wire was soldered to the contacting surface and the electrodes were mounted into the appropriate glass holder with epoxy resin.

Electrochemical measurements were performed in a 1 *M* NaOH electrolyte using a platinum counterelectrode and a saturated calomel reference electrode (SCE). Electrode potentials were controlled with a PRT 20-2X Tacussel potentiostat and a GSTP Tacussel programmer.

The light source was a 150-W high-pressure xenon lamp. The photon flux reaching the electrode surface had been determined with a calibrated EG&G 4000B silicon photovoltaic detector at each wavelength.

Impedance measurements of the cell, $Fe_{2.036}Ti_{0.964}O_4$/electrolyte/Pt, were made in the frequency range 1 Hz to 200 kHz using a Solartron 1174 transferometer.

Results and Discussion

Electrical Properties

Figure 1 shows the temperature dependence of the electrical conductivity. It provides clear evidence of two different temperature ranges.

For such iron–titanium spinels an elec-

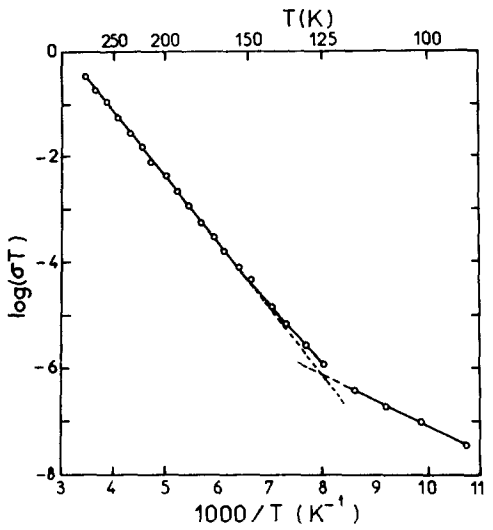

FIG. 1. Temperature dependence of the electrical conductivity of $Fe_{2.036}Ti_{0.964}O_4$.

tron hopping model is appropriate (*16*). In such a model the conductivity is given by the expression

$$\sigma = (\sigma_0/T)\exp(E_\sigma/kT) \qquad (1)$$

where k is the Boltzmann constant, σ_0 is a constant depending on composition, and E_σ is the activation energy of the conduction. In the high-temperature range ($T > 125$ K) $\log \sigma T$ exhibits, as expected, a linear variation characterized by constant energy (E_σ = 0.24 eV).

According to Mason and co-workers (*19*), the hopping mechanism occurs in titanomagnetite, as in all other ferrospinels, in octahedral sites between Fe^{3+} and Fe^{2+} ions.

Using the model developed by O'Neill and Navrotsky (*20*) and assuming that it can be extrapolated from 600°C down to room temperature and below, the corresponding extended formulas for our sample can be written as

298 K $Fe^{2+}_{0.953}Fe^{3+}_{0.047}(Fe^{2+}_{1.011}Fe^{3+}_{0.025}Ti^{4+}_{0.964})O_4$
250 K $Fe^{2+}_{0.944}Fe^{3+}_{0.056}(Fe^{2+}_{1.020}Fe^{3+}_{0.016}Ti^{4+}_{0.964})O_4$
220 K $Fe^{2+}_{0.938}Fe^{3+}_{0.062}(Fe^{2+}_{1.026}Fe^{3+}_{0.010}Ti^{4+}_{0.964})O_4$

On the other hand, at low temperature ($T <$ 125 K) the conductivity probably corresponds to an extrinsic region in which the charge carriers result from some nonstoichiometric defects.

The thermal dependence of the Seebeck coefficient is reproduced in Fig. 2. The sign of θ is positive in the temperature range investigated and the small activation energy of thermopower (E_θ = 0.02 eV) is consistent with the hopping mechanism; however, the sign of θ does not necessarily involve a p-type character since one is dealing with electron hopping occurring through the common edge of the octahedra from the $Fe^{2+}:t_{2g\beta}$ level to the (empty) $Fe^{3+}:t_{2g\beta}$ level, which would illustrate rather an n-type character. The corresponding value of θ is given by (*19*)

$$\theta = -\frac{k}{e}\left\{\ln 2\,\frac{[Fe^{3+}_{oct}]}{[Fe^{2+}_{oct}]} + A\right\} \qquad (2)$$

under the assumption that only one mobile electron is permitted on a given site and that all other interaction effects can be

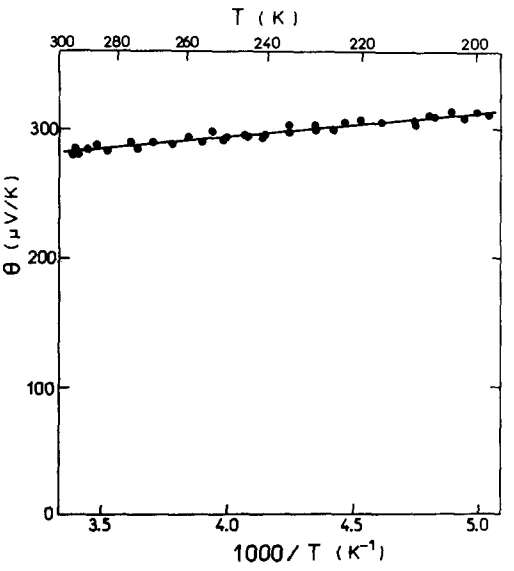

FIG. 2. Temperature dependence of the thermoelectric power of $Fe_{2.036}Ti_{0.964}O_4$.

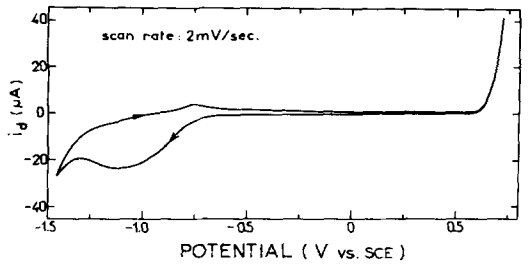

FIG. 3. Cyclic voltammograms of a $Fe_{2.036}Ti_{0.964}O_4$ electrode in a 1 *M* NaOH solution. Scanning rate: 2 mV/sec.

neglected (*19, 21*); the constant *A* involving the entropy of transport can be neglected for a small polaron conduction.

According to Eq. (2) and Fig. 2 the following θ values have been deduced:

T (K)	298	250	220
θ_{calc} (μV/K)	+ 259.1	+ 298.7	+ 341.4
θ_{exp} (μV/K)	+ 289	+ 295	+ 305

We must take into account that although experimental and calculated values are in good agreement, one cannot deduce the conductivity type. In fact, the *n*-type conductivity previously suggested will be confirmed on the basis of photoelectrochemical and capacitance measurements.

Current–Potential Characteristics

Figure 3 shows cyclic voltammograms between −1.40 and 0.70 V at a scan rate of 2 mV/sec. The dark currents (i_d) are less than 2 μA in the potential range $-0.6 < V < 0.6$ V, showing a small anodic peak near −0.75 V (curve 1). A large rise in i_d above 0.6 V corresponds to the oxygen evolution, as gas bubbles are noticeable on the electrode surface. In addition, relatively large cathodic dark currents near −1 V in curve 2 can be attributed to the reduction of dissolved oxygen, although the reduction of the electrode itself cannot be neglected.

Figure 4 shows the chopped photoresponse of the electrode versus potential (full output of the Xe lamp). These data have been obtained by slowly scanning the potential from cathodic to anodic regions and chopping the light on and off regularly. The cathodic photocurrent is negligible even at quite negative potentials, whereas the anodic photocurrent is large under positive polarization ($V > 0$ V); this is consistent with an *n*-type character.

Action Spectrum and Bandgap

The photocurrent wavelength spectrum has been measured between 270 and 550 nm at 0.6 V. Quantum efficiencies (η) were calculated by dividing the electron flow in the external circuit by the photon rate at each wavelength without correcting for reflectance effects. As shown in Fig. 5 the deduced η values are quite low (less than 4%).

According to the Gärtner model (*22*) the energy gap (*Eg*) of indirect transitions can be determined by plotting $[-h\nu \ln(1-\eta)]^{1/2}$ vs $h\nu$. As shown in Fig. 6, the $[-h\nu \ln(1-\eta)]^{1/2}$ vs $h\nu$ graph consists of two parts. The intercept of part I in curve a with the $h\nu$ axis gives the energy gap $Eg_1 = 2.00 \pm 0.02$

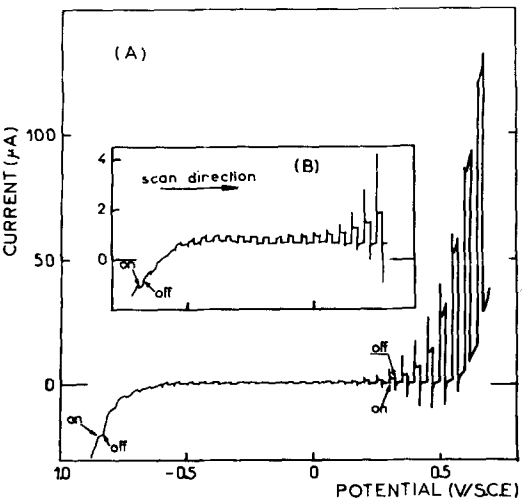

FIG. 4. Chopped photocurrent vs potential curves of the $Fe_{2.036}Ti_{0.964}O_4$ electrode under chopped light illumination. Scanning rate: 1 mV/sec.

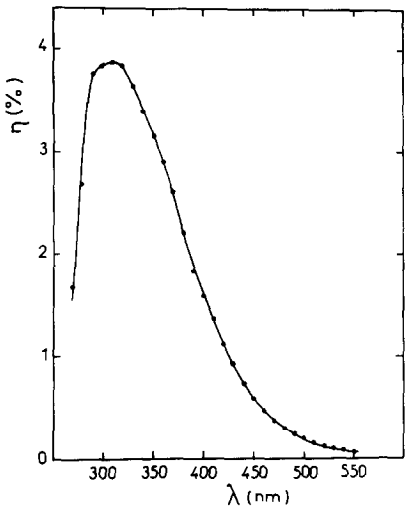

FIG. 5. Spectral dependence of the quantum efficiency of photocurrents at 0.6 V.

eV. In this region ($\lambda > 500$ nm), the quantum efficiencies (η_1) are less than 0.002.

For $h\nu > Eg_2$ the total quantum efficiency is the sum of η_1 and η_2. Since the variation of η_1 in the region $h\nu > Eg_2$ is known, only upper and lower limits of Eg_2 can be deduced from the data (*23*). The lower limit of Eg_2 obtained by extrapolation is 2.30 eV from part II of curve a, while the upper limit of 2.48 eV can be obtained from the deduced $-h\nu \ln[1 - (\eta - \eta_1)]\}^{1/2}$ vs $h\nu$ plots (curve b). Consequently, one can express it as $Eg_2 = 2.39 \pm 0.09$ eV.

Semiconductor–Electrolyte Interface Capacitance: Flatband Potential Determination

As is well known, the space charge capacitance (C_{sc}) of a semiconductor in contact with an electrolyte can be used to determine V_{fb} according to the Mott–Schottky equation (*24*)

$$C_{sc}^{-2} = 2(\varepsilon\varepsilon_0 q_0 N)^{-1}(V - V_{fb} - kT/q_0) \quad (3)$$

where N is donor or acceptor concentration, and ε and ε_0 are dielectric constants of the semiconductor and the vacuum, respectively.

For $V > -0.5$ V the dark current is very low, so that the space charge capacitance (C_{sc}) can be obtained in this potential region and lead to an accurate V_{fb} determination from the Mott–Schottky equation.

Electrode–electrolyte interface impedances were measured as a function of potential at -0.6 V $< V < 0.4$ V in the frequency range 1 Hz to 200 kHz, and permittivity diagrams were deduced from these measurements. For a simple circuit composed of a resistor and a capacitor in series the permittivity diagram gives a perfect semicircle: its intercept with the real axis corresponds to the value of the capacitance. The diagrams in Fig. 7 show actually only slightly inclined semicircular arcs in the high-frequency region. The corresponding diameters decrease with increasing potential; however, we have retained the intercept with the real axis as an appropriate value of the space charge capacity.

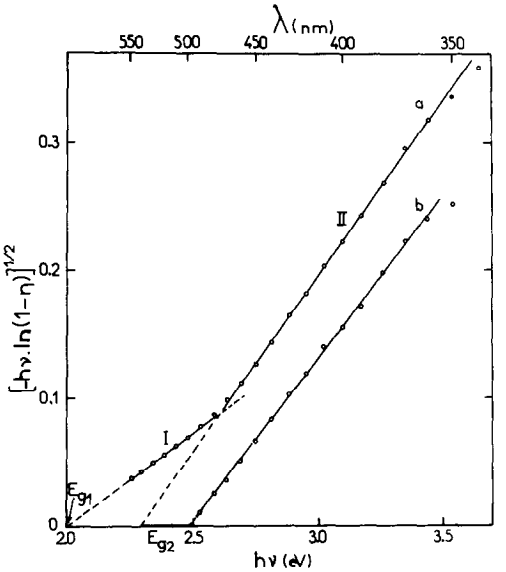

FIG. 6. Curve a: $[-h\nu \ln(1 - \eta)]^{1/2}$ vs $h\nu$ plots deduced from Fig. 5. See the text for the meaning of curve b.

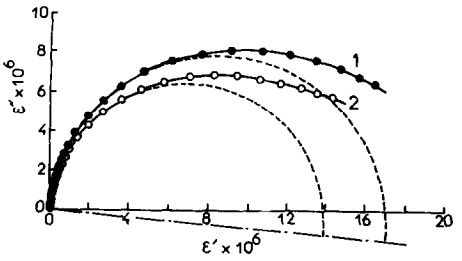

FIG. 7. Permittivity diagrams of the electrode–electrolyte interface deduced from impedance measurements. Curve 1: 0.0 V, curve 2: 0.4 V.

The deduced C_{sc} values are plotted versus potential (Fig. 8). The linear part leads to the extrapolated flatband potential (V_{fb}). The obtained $V_{fb} = -0.65$ V determination is in good agreement with the onset of the current–potential characteristics (Fig. 4). Such a negative V_{fb} value provides unambiguous evidence of *n*-type character.

Electronic Transition in Titanium-Rich Titanomagnetite

The previous electronic studies of Fe_2TiO_4 have clearly shown that this compound has typically the behavior of an inverse spinel-type material (*24*). Therefore, the energy diagram of Fe_2TiO_4 can be referred to that of Fe_3O_4 except for the influence of Ti^{4+} ions on the octahedral sites.

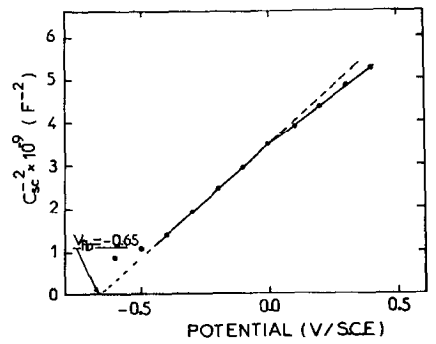

FIG. 8. Mott–Schottky plots of a $Fe_{2.036}Ti_{0.964}O_4$ electrode in a 1 *M* NaOH solution.

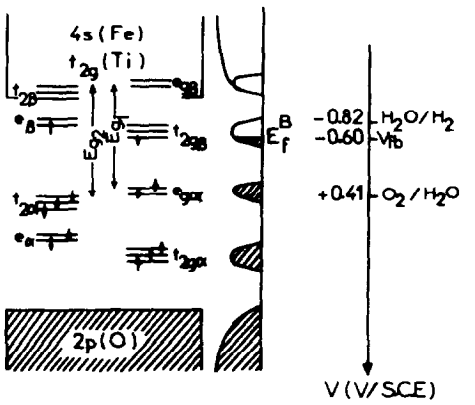

FIG. 9. Schematic energy level diagram of $Fe_{2.036}Ti_{0.964}O_4$ (pH 13.8). (A) Tetrahedral site. (B) Octahedral site.

Concerning the electronic structure of the magnetite Fe_3O_4 several models have been proposed (*25–28*). According to those models, it exhibits two wide bands of filled 2*p* oxygen and empty 4*s* iron character which are separated by an energy gap of 5–6 eV. On the other hand, the iron 3*d* electrons strongly interact with each other and with the surrounding oxygen anions to form more or less localized states in the energy gap.

The proposed energy diagram for Fe_2TiO_4 is given in Fig. 9. For Fe_3O_4 the highest-lying 3*d* state in the octahedral sites of $Fe^{2+}_{oct}(t_{2g}^4 e_g^2)$ is placed 0.5–0.6 eV below the bottom of the 4*s* band (*27*), and $t_{2g\beta}$ levels contribute to its electrical conductivity. On the other hand, the electrical conduction of our titanomagnetite results from charge transfer between neighboring Fe^{2+} and Fe^{3+} ions in the surrounding octahedra and the activation energy is found to be 0.24 eV (Table I).

As shown in Fig. 9 the Fermi level of the titanomagnetite should be correlated to the $t_{2g\beta}$ level, corresponding to the flat-band potential of -0.65 ± 0.05 V vs SCE at pH 13.8. In addition, the empty energy levels of Ti^{4+} must lie above the e_β or $t_{2g\beta}$ levels of

TABLE I

PHYSICAL PROPERTIES OF $Fe_{2.036}Ti_{0.964}O_4$

Conductivity at 300 K (Ω^{-1} cm^{-1})	1.5×10^{-3}
Activation energy for conductivity (eV)	
$T > 125$ K	0.24
$T < 125$ K	0.10
Flatband potential at pH 13.8 (V vs SCE)	−0.65
Interband indirect transition energy (eV)	
Eg_1	2.00
Eg_2	2.39

iron ions, as titanium always occurs under stable conditions as Ti^{4+} cation in titanomagnetite.

We can reasonably conclude from the preceding discussion that the splitting between $2p(O^{2-})$ and $3d(Fe^{3+}$ or $Ti^{4+})$ levels is too large (more than 4 eV) to explain the observed optical transition energies (Eg_1 = 2.00 eV and Eg_2 = 2.39 eV). If we reasonably exclude any Fe^+ formation, even with a delocalized electron in the 4*s* band, the most probable electronic charge transfer involving electron-hole pair creation that can be expected is as follows:

For Eg_1

$$Fe^{2+}_{oct}(e^2_{g\alpha}) + Fe^{3+}(4s^0) \rightarrow Fe^{3+}_{oct}(e^1_{g\alpha}) + Fe^{2+}(4s^1) \quad (4)$$

or (and) eventually

$$Fe^{2+}_{oct}(e^2_{g\alpha}) + Ti^{4+}(3d^0) \rightarrow Fe^{3+}(e^1_{g\alpha}) + Ti^{3+}(3d^1). \quad (5)$$

For Eg_2

$$Fe^{2+}_t(t^3_{2\alpha}) + Fe^{3+}(4s^0) \rightarrow Fe^{3+}_t(t^2_{2\alpha}) + Fe^{2+}(4s^1) \quad (6)$$

or (and) eventually

$$Fe^{2+}_t(t^3_{2\alpha}) + Ti^{4+}(3d^0) \rightarrow Fe^{3+}_t(t^2_{2\alpha}) + Ti^{3+}(3d^1). \quad (7)$$

Thus the photocurrent in $Fe_{2.036}Ti_{0.964}O_4$ should result mainly from iron–iron electron transfers, but the contribution of iron–titanium charge transfer should not be neglected. It takes place mainly in the tetrahedral cation sublattice.

Let us point out that the localized energy levels of iron ions, leading to low mobility of the photogenerated holes, are responsible for the weak photocurrent observed (Fig. 4) particularly for negative potentials.

Conclusion

Besides the electronic properties investigated by conductivity and thermoelectric power measurements, some other features of the electronic structure have been determined from the photoelectrochemical behavior of our ulvospinel. As expected the small energy gaps Eg_1 (2.00 eV) and Eg_2 (2.39 eV) observed from $[-h\nu \ln(1 - \eta)]^{1/2}$ vs $h\nu$ plots should be attributed to Fe–Fe electronic transitions; however, Fe–Ti charge transfer cannot be fully excluded. According to our model the Fe–Fe electronic transitions occurring in both octahedral and tetrahedral sites are responsible for the anodic photoresponse (*n* character). The flatband potential determined from the impedance measurements is close to that observed for *n*-type α-Fe_2O_3 (*5*); therefore the presence of Ti in the ulvospinel does not seem to contribute to a reduction of the electron affinity of the semiconductor.

Acknowledgment

These investigations have been supported by GRECO 130061 of the CNRS.

References

1. K. L. HARDEE AND A. J. BARD, *J. Electrochem. Soc.* **123,** 1024 (1976).
2. R. K. QUINN, R. D. NASBY, AND R. J. BAUGHMAN, *Mater. Res. Bull.* **11,** 1011 (1976).
3. J. H. KENNEDY AND M. ANDERMAN, *J. Electrochem. Soc.* **130,** 848 (1983).
4. D. E. SCAIFE, *Solar Energy* **25,** 41 (1980).
5. J. H. KENNEDY AND K. W. FRESE, *J. Electrochem. Soc.* **125,** 723 (1978).
6. M. P. DARE-EDWARDS, J. B. GOODENOUGH, A.

HAMNETT, AND P. R. TREVELLIK, *J. Chem. Soc. Faraday Trans. 1* **79,** 2027 (1983).
7. M. V. C. SASTRI AND G. NOGASUBRAMANIAN, *Int. J. Hydrogen Energy* **7,** 873 (1982).
8. J. E. TURNER, M. HENDEWERK, J. PARMETER, D. NEIMAN, AND G. A. SOMORJAI, *J. Electrochem. Soc.* **131,** 1777 (1984).
9. K. ITOH AND J. O'M. BOCKRIS, *J. Electrochem. Soc.* **131,** 1266 (1984).
10. H. MORISAKI, H. ONO, H. DOHKOSKI, AND K. YAZAWA, *Japan. J. Appl. Phys.* **19,** L148 (1980).
11. F. T. LIOU AND C. Y. YANG, *J. Electrochem. Soc.* **129,** 342 (1982).
12. G. NOGAMI, *Denki Kagaku* **50,** 309 (1982).
13. T. OSAKA, K. EJIRI, AND N. HIRATA, *J. Electrochem. Soc.* **131,** 1571 (1984).
14. B. MOROSIN, R. J. BAUGHMAN, D. S. GINLEY, AND M. A. BUTLER, *J. Appl. Crystallogr.* **11,** 121 (1978).
15. D. S. GINLEY AND M. A. BUTLER, *J. Appl. Phys.* **48,** 2019 (1977).
16. S. K. BANERJEE, W. O'REILLY, T. C. GIBB, AND N. N. GREENWOOD, *J. Phys. Chem. Solids* **28,** 1323 (1967).
17. R. ARAGON, H. R. HARRISON, R. H. MCCALLISTER, AND C. J. SANDBERG, *J. Cryst. Growth* **61,** 221 (1983).
18. P. DORDOR, E. MARQUESTAUT, AND G. VILLENEUVE, *Rev. Phys. Appl.* **15,** 1607 (1980).
19. A. TRESTMANN-MATTS, S. E. DORRIS, S. KUMARAKRISHNAN, AND T. O. MASON, *J. Amer. Ceram. Soc.* **66,** 829 (1983).
20. H. S. C. O'NEIL AND A. NAVROTSKY, *Amer. Mineral.* **68,** 181 (1983).
21. H. L. TULLER AND A. S. NOWICK, *J. Phys. Chem. Solids* **38,** 859 (1977).
22. W. W. GÄRTNER, *Phys. Rev.* **116,** 84 (1959).
23. E. POLLERT, J. HEJTMANEK, J. P. DOUMERC, J. CLAVERIE, AND P. HAGENMULLER, *J. Phys. Chem. Solids* **44,** 273 (1983).
24. F. MOLLERS, H. J. TOLLE, AND R. MEMMING, *J. Electrochem. Soc.* **121,** 1160 (1974).
25. Y. ISHIKAWA, S. SATO, AND Y. SYONO, *J. Phys. Soc. Japan* **31,** 452 (1974).
26. D. L. CAMPHAUSEN, J. M. D. COEY, AND B. K. CHAKRAVERTY, *Phys. Rev. Lett.* **29,** 657 (1972).
27. I. BALBERG AND H. L. PINCH, *J. Magn. Magn. Mater.* **7,** 12 (1978).
28. A. SCHLEGEL, S. F. ALVARADO, AND P. WACHTER, *J. Phys. C* **12,** 1157 (1979).